PHYSICAL REVIEW B **85**, 041301(R) (2012)

Room-temperature continuous wave lasing in deep-subwavelength metallic cavities under electrical injection

K. Ding,[1] Z. C. Liu,[1] L. J. Yin,[1] M. T. Hill,[2] M. J. H. Marell,[2] P. J. van Veldhoven,[2] R. Nöetzel,[2] and C. Z. Ning[1,*]

[1] *School of Electrical, Computer, and Energy Engineering, Arizona State University, Tempe, Arizona 85287, USA*

[2] *COBRA Research Institute, Technische Universiteit Eindhoven, NL-5600 MB Eindhoven, The Netherlands*

(Received 26 July 2011; published 4 January 2012)

Plasmonic nanolasers and spasers continue to attract a great deal of interest from the physics and nanophotonics community, with the experimental observation of lasing as a focus of research. We report the observation of continuous wave lasing in metallic cavities of deep subwavelength sizes under electrical injection, operating at room temperature. The volume of the nanolaser is as small as $0.42\lambda^3$, where $\lambda = 1.55\ \mu$m is the lasing wavelength. This demonstration will help answer the question of how small a nanolaser can be made, and will likely stimulate a wide range of fundamental studies in basic laser physics and quantum optics on truly subwavelength scales. In addition, such nanolasers may lead to many potential applications, such as on-chip integrated photonic systems for communication, computing, and detection.

DOI: 10.1103/PhysRevB.85.041301 PACS number(s): 78.67.−n, 42.55.Px, 42.55.Sa, 81.07.−b

Nanoscale metal-dielectric composite structures have been a subject of ever growing interest in many fields of study such as plasmonics, metamaterials, nanophotonics, nanolasers, and quantum optics. A wide array of interesting phenomena has been predicted or observed. One of the most fundamental issues for all these applications is heating-related metal loss. Thus replacing dielectric materials with gain media such as semiconductors has been considered one of the key options to compensate for metal loss and to eventually enable the realization or observation of these predicted phenomena. An important related question is if the gain medium is capable of overcompensating for metal loss[1] at room temperature (RT), thus allowing RT operation of spasers[1,2] or plasmonic nanolasers, especially under electrical injection. Spasers and plasmonic nanolasers with deep subwavelength cavities represent one of the important frontiers of research in nanophotonics and nanotechnology in general.[1–10] While metals have been used as parts of the laser cavity for long wavelengths,[11] it remains an open question if metals such as silver or gold can be used to make a subwavelength cavity in the near infrared or shorter wavelength, due to dramatically increased metal loss in these wavelengths, especially at RT.[12] Theoretical studies[10,13] that accounted for wavelength compression and metal loss near surface plasmon polariton (SPP) resonance showed that it was indeed possible to realize a net positive gain in a semiconductor-metal core-shell structure. This was soon verified in an experiment with a semiconductor-metal core-shell structure.[3] While great progress has been made in the past few years in nanolasers with deep subwavelength-sized metal cavities[1–8] and spacers,[2,9] the realization of RT continuous wave (cw) operation under electrical injection has remained elusive. Despite intensive activities worldwide, subwavelength-cavity RT lasing has been demonstrated only under optical[5–7] or electrical-pulse pumping,[4] or under cw electrical pumping but at low temperature.[4] RT cw lasing under electrical injection has been observed only for a metallic cavity that is larger than the wavelengths.[14] Since optical pumping can be a near-resonant process with minimum heat generation, the fundamental question remains as to if a metallic subwavelength laser can work at room temperature under electrical injection, which is eventually necessary for any practical applications.

The research into truly nanoscale subwavelength lasers is also part of a long-term endeavor aimed at answering some fundamental questions of laser physics and quantum optics, such as the following:[10] Is there a fundamental size limit to a nanolaser? What is that limit if there is? Size reduction of semiconductor lasers have in the past enabled studies of many rich physics on an ever decreasing spatial scale and the development of many technological applications. The quantum optics and laser physics community has witnessed dramatic progress over the past few decades in making increasingly smaller lasers using pure dielectric structures such as microdisk lasers,[15–17] photonic wire lasers,[18] photonic crystal (PC) lasers,[19–22] or nanowire lasers.[10,23–26] These lasers represented the smallest lasers made of pure dielectric structures, and further miniaturization becomes exceedingly challenging. Size reduction to true nanoscales encounters a fundamental roadblock imposed by the wavelength involved and the poor confinement of optical modes.[10] The ideas and concepts around spasers[1,2] and plasmonic nanolasers provide important incentives for this pursuit.

This Rapid Communication reports subwavelength metallic-cavity nanolasers operating at room temperature under cw electrical injection. Our devices consist of an InP/InGaAs/InP pillar etched from a wafer grown by metalorganic chemical vapor deposition (MOCVD) with a 20-nm Si_3N_4 layer on all four sides, as shown in Fig. 1(a). The device layer forms a three-layer sandwich waveguide in the vertical (z) direction with an index profile of 3.1(InP)/3.4(InGaAs)/3.1(InP), confining light mostly in the InGaAs. This pillar is then encapsulated in silver from all four sides and the top, forming a metal-insulator-semiconductor-insulator-metal (MISIM) waveguide in the horizontal (x and y) directions.[27]

Four devices were measured and reported on in the following, as listed in Table I. Emission is collected from the backside of the substrate [as indicated in Fig. 1(b)] by an objective lens and detected by a spectrometer equipped with a liquid-nitrogen-cooled InGaAs array detector.[27] The

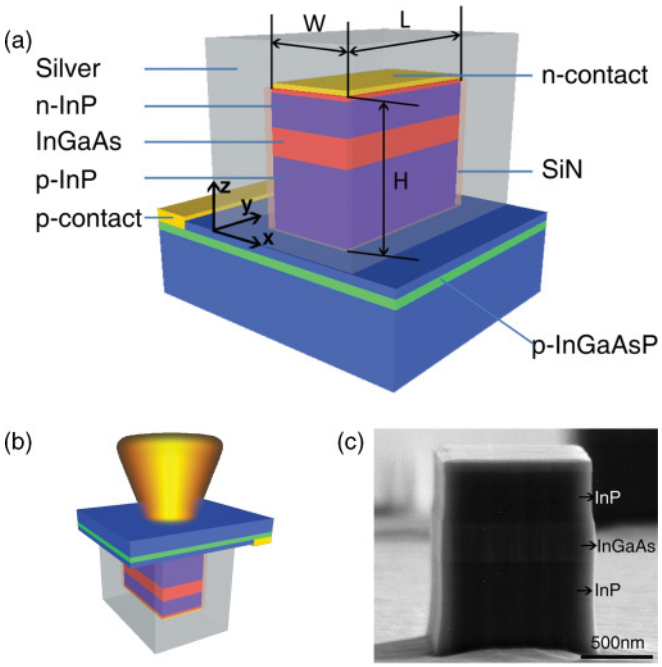

FIG. 1. (Color online) (a) Semiconductor pillar of a rectangular cross section is encapsulated in silver to form a metallic cavity. (b) Schematic of a laser structure inverted showing laser light emitted from the backside of the substrate. (c) Scanning electron microscope image showing the semiconductor pillar before SiN and silver coating.

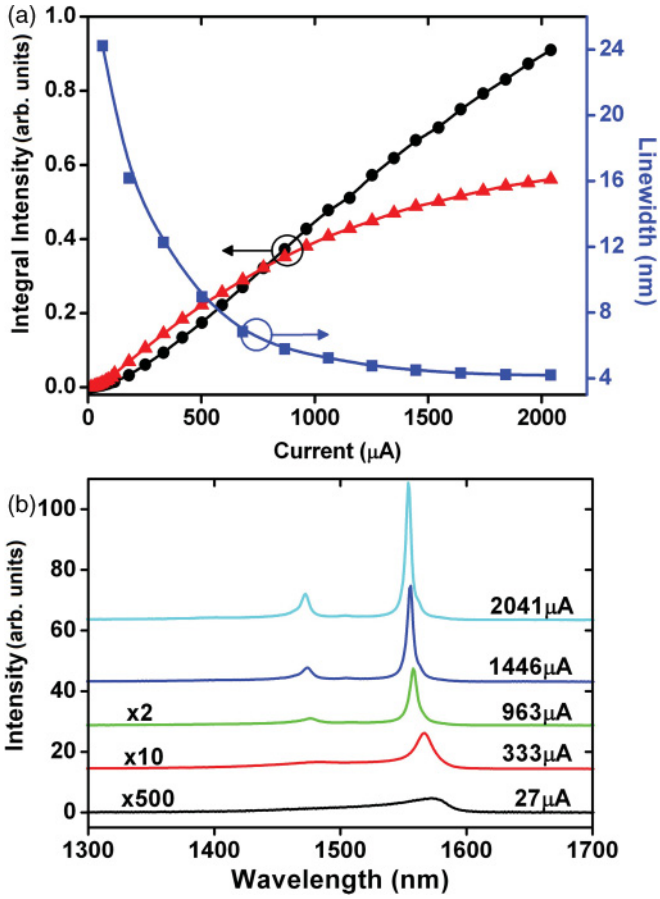

FIG. 2. (Color online) (a) Linewidth (FWHM, ■ squares), integrated lasing mode intensity (● circles), and integrated spontaneous emission intensity (▲ triangles), as functions of dc current at 293 K. The threshold is estimated ∼1000 μA. (b) Spectra at different dc currents (offset for clarity).

light output versus current (L-I) curve for device 1 with a volume of $0.42\lambda^3$ is shown in Fig. 2(a). The threshold current is estimated to be ∼1000 μA. The integrated spontaneous emission shows a slower increase and then saturation starts to set in with an increase of injection current, indicating carrier density pinning (somewhat weakly) in the active region, which is an important signature of lasing. The full width at half maximum (FWHM) of the lasing mode shows a rapid decrease first with increasing current and then a gradual saturation to ∼4 nm at 2.04 mA. Such a linewidth behavior is also typical of a laser transition from below to above threshold as the pumping increases. As shown in Fig. 2(b), the lasing peak blueshifts from 1568 nm well below threshold to 1554 nm at 2.04 mA. At a higher injection current, another lasing peak at 1471 nm emerges.[27] The mode spacing of 83 nm gives a group index of 4.59 by using the standard formula $n_g = \frac{\lambda_1\lambda_2}{2L(\lambda_1-\lambda_2)}$, where L is the length of the device. Such a high group index is due to the combination of high modal plasmonic dispersion of the waveguide and significant material dispersion. A group index of 4.15 or 4.62 is calculated without or with material dispersion $\partial\varepsilon_r/\partial\omega \sim 4 \times 10^{-15}$ s (Ref. 28) of InGaAs, in good agreement with experiment results. Both the group index and the cavity length indicate that the modes correspond to the cavity along the y direction (see Fig. 1).

TABLE I. List of devices reported in the paper.

Device No.	Width (μm)	Length (μm)	Height (μm)	Volume (λ^3)
1	0.34	3	1.53	0.42
2	1.1	2.15	1.55	0.95
3	0.28	6	1.53	0.71
4	0.9	2.1	1.55	1.01

Generally, larger devices exhibit narrower FWHM at room temperature. Device 2 has a larger volume at $0.95\lambda^3$ and its operation characteristics are shown in Fig. 3, where the intensity of the lasing mode is plotted in comparison with a nonlasing mode and spontaneous emission [Fig. 3(a)]. We see a much weaker increase in spontaneous emission. The nonlasing mode competes with the lasing mode initially, but eventually saturates to give way to lasing. The FWHM decreases from 6.5 nm well below threshold to 3 nm at 1.57 mA at 293 K under dc current injection [Fig. 3(a)]. Figure 3(b) shows the linewidth dependence on current at different temperatures. As the temperature increases, the linewidth saturation becomes weaker and at higher values. Several known physical effects are responsible for such a linewidth increase with temperature, including elevated carrier density and a higher active region temperature. The higher threshold leads to more heat generation. The increased temperature leads to higher nonradiative recombination and decreased gain, which further increases the

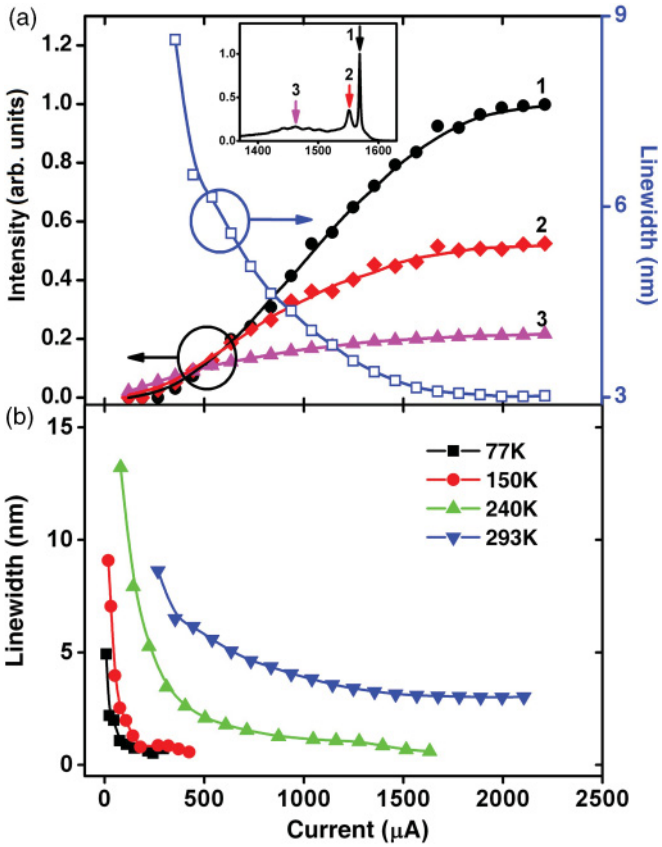

FIG. 3. (Color online) (a) Light intensity and FWHM as functions of dc current at 293 K. Inset: Spectrum with arrows and numbers indicating positions where the light intensity is taken: lasing mode (● circles, 1), nonlasing mode (◆ diamonds, 2), and spontaneous emission at 1460 nm (▲ triangles, 3). The threshold is estimated ∼1000 μA. (b) FWHM at different temperatures.

threshold current. Such negative feedback between increased heating and required higher injection current is the main reason for the linewidth increase with temperature. The linewidth of a laser is proportional to $(1+\alpha^2)/P$.[29,30] P is the laser power and α is the linewidth enhancement factor. Due to the higher carrier density required at RT, α is significantly larger than at low density.[31] Since the device cannot be pumped very far above the threshold at RT due to the increased threshold and thermal effect, the output power is significantly lower. A smaller output power and a larger α both lead to a larger linewidth. We believe that a significant improvement in heat dissipation can lead to a much reduced linewidth in the future.

To shed more light on the modal properties of nanocavity lasers, mode patterns and polarization properties are studied by a combination of experimental measurement and simulation for two more devices (devices 3 and 4) at 100 K, as shown in Fig. 4. Two modes from each device were studied at $\lambda_1 =$ 1532 nm (mode 1, or M1) and $\lambda_2 = 1540$ nm (mode 2 or M2) for device 3 and $\lambda_1 = 1428$ nm (M1) and $\lambda_2 = 1433$ nm (M2) for device 4. Polarization-resolved light intensity for these two modes is shown in Figs. 4(j) and 4(k), respectively. The maxima of the polarized intensity are in the y direction (zero-degree angle in the figure) for M1 of both devices, while M2 shows a roughly opposite behavior with the minimum shifted by ∼20° from the maximum of M1. The large contrast of M1 for device 3 indicates that the light output is a predominantly linearly polarized along one direction, while M1 for device 4 is less polarized with a smaller contrast. This is consistent with the aspect ratio of the x-y cross sections of the two devices. Simulations using COMSOL found two modes at 1550 and 1565 nm for device 3, in agreement with the experimental values. The near-field patterns in Figs. 4(a)–4(d) for M1 and Figs. 4(e)–4(h) for M2 show that M1 is mostly confined in the gain medium and is dominated by E_z, while M2 is mostly in the dielectric gap and is dominated by E_x. The far field of M1 and M2 was calculated using an equivalent surface approach[32] and is shown to be dominated by E_y and E_x, respectively, consistent with the experimental measurements shown in Figs. 4(j) and 4(k). The L-I curve of device 3 [Fig. 4(i)] shows that M1 eventually becomes a lasing mode, while M2 saturates after the threshold. This can be understood from the simulation, since M1 is mostly confined in the gain medium with a much bigger confinement factor[33,34] than M2. The consistency between the experimental and simulation results further validates our overall understanding of the features of the nanolasers. Based on the similarity between devices 1 and 3 and between devices 2 and 4, we expect that the lasing modes discussed previously for devices 1 and 2 are M1-like, both with significant E_x and E_z components. The E_z component is approximately three times larger than E_x. If one associates E_x and E_z with plasmonic and photonic modes, respectively, then the lasing modes are likely to be mixtures with a larger photonic component.

In summary, we demonstrate cw RT lasing under electric injection in two of the metallic cavity lasers with a total volume that is smaller than λ^3. Currently the device performance is still limited by significant heating. Improvement of the device design and optimization of the thermal packaging are key factors for further improvements in device performance. Since metallic cavities provide a much smaller physical separation between the active regions and the metals than do traditional dielectric cavity devices, we believe that future generations of devices will allow much improved heat dissipation and device performance.

Our results represent an important step in the development of nanolasers with a deep subwavelength volume and pave the way for many practical applications of nanolasers, such as on-chip integrated optical interconnects for future computing and communications, and for on-chip integrated detection and sensing systems. From a fundamental physics point of view, our results show that metal loss can be overcome by a semiconductor gain medium even at room temperature, under cw electrical injection, and in the near-infrared wavelengths. Since metallic structures are indispensable for many interesting physics phenomena in metamaterials, active plasmonics, spasers, and subwavelength nanolasers, it is fundamentally important to demonstrate that metal loss can be overcompensated for under realistic conditions. Thus these results will impact all these areas where composites of metallic and semiconductor structures are required, since heating-related metal loss has been a major deciding factor for all these applications. In addition, deep subwavelength lasers will

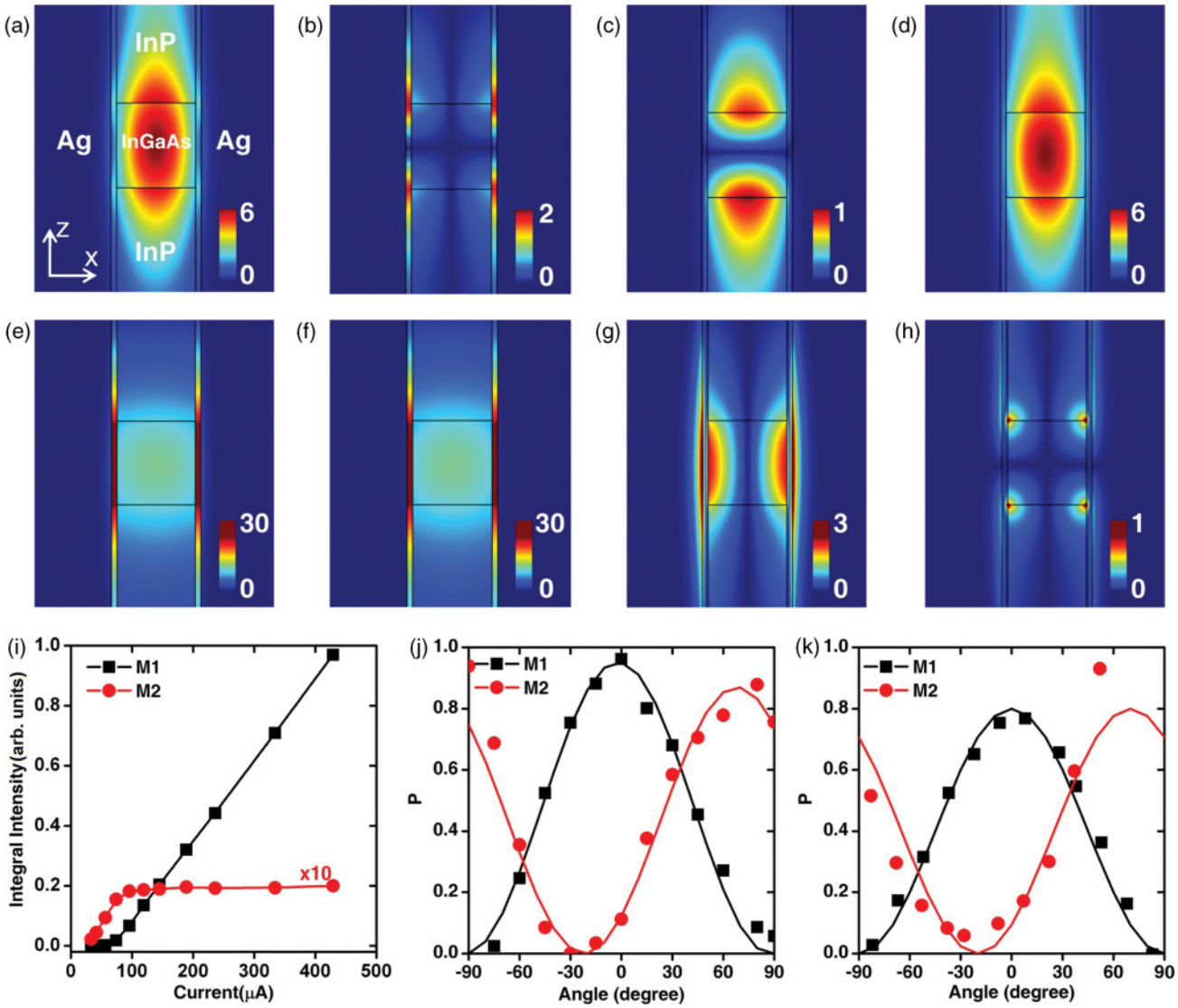

FIG. 4. (Color online) Modal and polarization properties for devices 3 and 4. Simulated $|E|$, $|E_x|$, $|E_y|$, and $|E_z|$ for mode 1 [M1, (a)–(d) and for mode 2 [M2, (e)–(h)], respectively, of device 3. L-I curve for M1 and M2 of device 3 at 100 K (i). Polarization contrast [defined as $(I - I_{\min})/I_{\max}$] for M1 and M2 vs polarizer angle for device 3 (j) and for device 4 (k), where $I_{\max}$ and $I_{\min}$ are the maximum and minimum of modal intensity.

provide a different platform for the study of many fundamental issues in laser physics and quantum optics, just as microcavity lasers have done over the past two decades. Many interesting developments are expected in these fields.

The research is supported by the Defense Advanced Research Project Agency (W911NF-07-1-0314) and Air Force Office for Scientific Research (AFOSR, FA9550-10-01-0444)

*cning@asu.edu

[1]M. I. Stockman, Phys. Rev. Lett. **106**, 156802 (2011).

[2]D. J. Bergman and M. I. Stockman, Phys. Rev. Lett. **90**, 027402 (2003).

[3]M. T. Hill, Y. S. Oei, B. Smalbrugge, Y. Zhu, T. de Vries, P. J. van Veldhoven, F. W. M. van Otten, T. J. Eijkemans, J. P. Turkiewicz, H. de Waardt, E. J. Geluk, S. H. Kwon, Y. H. Lee, R. Nötzel, and M. K. Smit, Nat. Photonics **1**, 589 (2007).

[4]M. T. Hill, M. Marell, E. S. P. Leong, B. Smalbrugge, Y. Zhu, M. Sun, P. J. van Veldhoven, E. J. Geluk, F. Karouta, Y. S. Oei, R. Nötzel, C. Z. Ning, and M. K. Smit, Opt. Express **17**, 11107 (2009).

[5]R. F. Oulton, V. J. Sorger, T. Zentgraf, R. Ma, C. Gladden, L. Dai, G. Bartal, and X. Zhang, Nature (London) **461**, 629 (2009).

[6]M. P. Nezhad, A. Simic, O. Bondarenko, B. Slutsky, A. Mizrahi, L. Feng, V. Lomakin, and Y. Fainman, Nat. Photonics **4**, 395 (2010).

[7]K. Yu, A. Lakhani, and M. C. Wu, Opt. Express **18**, 8790 (2010).
[8]S. H. Kwon, J. H. Kang, C. Seassal, S. K. Kim, P. Regreny, Y. H. Lee, C. M. Lieber, and H. G. Park, Nano Lett. **10**, 3679 (2010).
[9]M. A. Noginov, G. Zhu, A. M. Belgrave, R. Bakker, V. M. Shalaev, E. E. Narimanov, S. Stout, E. Herz, T. Suteewong, and U. Wiesner, Nature (London) **460**, 1110 (2009).
[10]C. Z. Ning, Phys. Status Solidi B **247**, 774 (2010).
[11]C. Sirtori, C. Gmachl, F. Capasso, J. Faist, D. L. Sivco, A. L. Hutchinson, and A. Y. Cho, Opt. Lett. **23**, 1366 (1998).
[12]According to the Drude model, metal absorption is proportional to the resistivity, dominated by phonon scatterings which are stronger at RT than at low temperature. The resistivity increases by a factor of 5 from 77 to 273 K [see G. W. C. Kaye and T. H. Laby, *Table of Physical and Chemical Constants* (Longmans Green, London, 1966)]; Other measurements also showed an increased metal loss at higher photon energies above 2 eV [see R. H. M. Groeneveld, R. Sprik, and A. Lagendijk, Phys. Rev. Lett. **64**, 784 (1990)].
[13]A. V. Maslov and C. Z. Ning, Proc. SPIE **6468**, 64680I (2007).
[14]C. Y. Lu, S. W. Chang, S. L. Chuang, T. D. Germann, and D. Bimberg, Appl. Phys. Lett. **96**, 251101 (2010).
[15]A. F. J. Lev, S. L. McCall, S. J. Pearton, and R. A. Logan, IEEE Electron. Lett. **29**, 1666 (1993).
[16]T. Baba, P. Fujita, A. Sakai, M. Kihara, and R. Watanabe, IEEE Photonics Technol. Lett. **9**, 878 (1997).
[17]K. Srinivasan, M. Borselli, O. Painter, A. Stintz, and S. Krishna, Opt. Express **14**, 1094 (2006).
[18]J. P. Zhang, D. Y. Chu, S. L. Wu, S. T. Ho, W. G. Bi, C. W. Tu, and R. C. Tiberio, Phys. Rev. Lett. **75**, 2678 (1995).
[19]H. G. Park, S. H. Kim, S. H. Kwon, Y. G. Ju, J. K. Yang, J. H. Baek, S. B. Kim, and Y. H. Lee, Science **305**, 1444 (2004).
[20]K. Nozaki, H. Watanabe, and T. Baba, Appl. Phys. Lett. **92**, 021108 (2008).
[21]S. Tomljenovic-Hanic, C. M. de Sterke, M. J. Steel, B. J. Eggleton, Y. Tanaka, and S. Noda, Opt. Express **15**, 17248 (2007).
[22]A. J. Danner, J. C. Lee, J. J. Raftery, N. Yokouchi, and K. D. Choquette, Electron. Lett. **39**, 1323 (2003).
[23]M. H. Huang, S. Mao, H. Feick, H. Yan, Y. Wu, H. Kind, E. Weber, R. Russo, and P. Yang, Science **292**, 1897 (2001).
[24]R. Chen, T. T. D. Tran, K. W. Ng, W. S. Ko, L. C. Chuang, F. G. Sedgwick, and C. Chang-Hasnain, Nat. Photonics **5**, 170 (2011).
[25]R. Yan, D. Gargas, and P. Yang, Nat. Photonics **3**, 569 (2009).
[26]X. F. Duan, Y. Huang, R. Agarwal, and C. M. Lieber, Nature (London) **421**, 241 (2003).
[27]See Supplemental Material at http://link.aps.org/supplemental/10.1103/PhysRevB.85.041301 for details of device fabrication, optical measurement setup, longitudinal mode verification and simulation for device 1.
[28]S. J. Adachi, Appl. Phys. **66**, 6030 (1989).
[29]H. Haug and H. Haken, Z. Phys. **204**, 262 (1967).
[30]C. H. Henry, IEEE J. Quantum Electron. **18**, 259 (1982).
[31]C. Z. Ning, W. W. Chow, D. J. Bossert, R. A. Indik, and J. V. Moloney, IEEE J. Sel. Top. Quantum Electron. **3**, 129 (1997).
[32]C. A. Balanis, *Advanced Engineering Electromagnetics* (Wiley, New York, 1989), p. 329.
[33]A. V. Maslov and C. Z. Ning, IEEE J. Quantum Electron. **40**, 1389 (2004).
[34]D. B. Li and C. Z. Ning, Appl. Phys. Lett. **96**, 181109 (2010).